Thermodynamic Analysis of Spin Crossover in

Molecules and Solid State Materials with pySCO

†Department of Physics, University of Florida, Gainesville, Florida 32611

‡Center for Molecular Magnetic Quantum Materials, Gainesville, Florida 32611

E-mail: aalbaveramata@ufl.edu

Dated August 15, 2025

Abstract

The study of spin crossover phenomena in metal complexes is of significant im-

portance in chemistry and materials science, with implications for both theoretical

advancements and practical applications. Traditionally, the analysis of electronic struc-

ture outputs in this domain often involves labor-intensive ad hoc scripting that lacks

standardization and transferability. To overcome these challenges, we have developed

pySCO, a library designed to automate and simplify thermodynamic analyses for this

family of metal complexes, offering seamless integration with popular electronic struc-

ture codes. We feature a detailed case study on an Fe(II) metal complex to highlight the

robust capabilities offered by the library and provide insights into the spin transition

regimes for this material.

1

Introduction

Several molecular aggregates, $^{1-4}$ solutions, $^{5-7}$ or adsorbates $^{8-12}$ of coordination complexes with $3d^4$ to $3d^7$ metal cores may undergo spin crossover transitions if the average crystal field parameter, $10\,\mathrm{D}q$, competes in magnitude with the electron pairing energy for the d-electrons. $^{13-16}$ This makes possible the existence of two ground states that depend upon the strength of the crystal field. As a result, small external perturbations switch the metal complex to a low- or high-spin state. $^{17-20}$ These families of coordination adducts have been studied experimentally for nearly a century. The first report dates back to the works of Polanyi, 21 and of Cambi and Szegö 22 in 1931, and premiering descriptions of Fe(II) spin transitions by Baker and Bobonich in 1964, 23 and by König and Madeja in 1966. 24 Although the development of theoretical models pursuing description of the phenomenon fell behind by nearly four decades, with the earliest work by Wajnflasz in 1970. 25,26

It could be argued that a reason that hampered early developments of thermodynamic and microscopic models is, in part, that prediction of spin conversion curves from simple modeling considerations poses a major challenge.^{27–29} Given the relatively small energy interval for the spin gap, subtle changes to the composition of the ligands result in different transition profiles,^{30–36} emergence of polymorphs,^{37,38} or suppression of the spin conversion.³⁹ The resulting variations to the intra- and inter-molecular cooperative interactions thus affect noticeably the spin equilibrium.

From the perspective of practical computational efforts, on the other hand, the need to facilitate efficient high-throughput analyses is becoming progressively more relevant for large-scale data curation of spin crossover candidates. This allows to model, and eventually understand, how different chemical functional groups influence the physical chemical properties for these materials. Common electronic structure codes like Gaussian, ⁴⁰ NWChem, ⁴¹ Orca, ⁴² Vasp, ⁴³ Quantum Espresso, ⁴⁴ among others, offer parallelization advantages to achieve that purpose. However, post-treatment of output data most often still is done with ad hoc scripts crafted individually by different research groups. These are not read-

ily available to the public, transferable between different electronic structure codes, readily reproducible nor, typically, have they been validated or cross-checked.

In this work, we address the problem by introducing the development of pySCO, a python library for automated scalable workflows with minimum user input requirements. We showcase its use on an Fe(II) metal complex for the determination of the spin-crossover energy, transition temperature, thermal evolution of the magnetic susceptibility and diverse analyses of the Gibbs free energy with the inclusion of a phenomenological interaction parameter.

Thermodynamic Fundamentals in the Library

The spin switching phenomenon and its diverse conversion behaviors may be treated theoretically with several models, $^{25-29,45-53}$, among them, the basic fundamentals for the regular solution model 54,55 consist of assuming that the spin state mixture for a given molecular aggregate is distributed statistically and forms a regular solution. For a given material at constant pressure, the conversion from low to high spin is a thermal equilibrium between both spin configurations. The state function therefore is the Gibbs free energy G = H - T S, where H and S label the enthalpy and entropy for the system, respectively. Here, the largest contribution to G is the internal electronic energy for the low- and high-spin states, where a spin conversion energy no larger than $10 \text{ kJ} \text{ mol}^{-1}$ typically is expected for the spin crossover in molecules and materials.

The total electronic energy for each spin state is readily available from electronic structure computations, and may be read from the output files using the pySCO library as show in Scheme 1. The energy for the spin crossover conversion

$$\Delta E_{\rm sco} = E_{\rm HS} - E_{\rm LS} + \Delta E_{\rm zpe} \tag{1}$$

is calculated from the total energy difference between the high- (HS) and low-spin (LS) states, $E_{\rm HS}$ and $E_{\rm LS}$, respectively, plus the zero-point vibrational energy difference $\Delta E_{\rm zpe}$,

```
from pysco import read

# VASP outputs
low_spin = read.vasp( "low_spin_dir" )
high_spin = read.vasp( "high_spin_dir" )

# Orca output
low_spin = read.orca( "low_spin_file" )
high_spin = read.orca( "high_spin_file" )

# NWChem output
low_spin = read.nwchem( "low_spin_file" )
high_spin = read.nwchem( "low_spin_file" )

# Gaussian output
low_spin = read.nwchem( "high_spin_file" )

# Gaussian output
low_spin = read.gaussian( "low_spin_file" )
high_spin = read.gaussian( "low_spin_file" )
high_spin = read.gaussian( "high_spin_file" )
```

Scheme 1: Reading output files from the VASP, ORCA, NWCHEM or GAUSSIAN electronic structure codes.

to wit 56,57

$$\Delta E_{\text{zpe}} = N_A k_B \sum_{i \in \text{HS}} \frac{\theta_{\text{vib},i}}{2} - N_A k_B \sum_{i \in \text{LS}} \frac{\theta_{\text{vib},i}}{2}$$
 (2)

Here, N_A and k_B are Avogadro's number and Boltzmann's constant, respectively, and the vibrational temperature $\theta_{\text{vib},i} = h\nu_i/k_B$ is computed from the set of harmonic vibrational frequencies $\{\nu_i\}$ for each spin state.

As measured, spin-crossover is a cooperative behavior in a bulk molecular crystal. From that perspective, it is legitimate to consider a set of N weakly interacting molecules of which $N_{\rm HS}$ are in the high-spin state at temperature T. Therefore the relative high-spin is $n_{\rm HS} = N_{\rm HS}/N$, in terms of which the Gibbs free energy of an ideal solution model that includes the Gibbs free energy of the individual molecular spin states is

$$G = n_{\rm HS} G_{\rm HS} + (1 - n_{\rm HS}) G_{\rm LS} - T S_{\rm mix}$$
 (3)

On the assumption that the inter-molecular coupling has negligible dependence on those spin states, and that the ideal entropy of mixing, S_{mix} , in the thermodynamic limit is

$$S_{\text{mix}} = -k_B N_A (n_{\text{HS}} \ln[n_{\text{HS}}] + (1 - n_{\text{HS}}) \ln[1 - n_{\text{HS}}])$$
 (4)

Scheme 2: Calculation of the spin crossover energy $\Delta E_{\rm sco}$, and transition temperature $T_{1/2}$ for low- and high-spin states defined as in Scheme 1.

The equilibrium condition is thus obtained by minimizing G and calculating the associated maximum spin conversion,

$$\left(\frac{\partial G}{\partial n_{\rm HS}}\right)_{T,P} = 0
\tag{5}$$

Hence, the thermal evolution of $n_{\rm HS}$ is

$$T = \frac{\Delta H}{k_B N_A \ln\left[\frac{1 - n_{\rm HS}}{n_{\rm HS}}\right] + \Delta S} \tag{6}$$

with the extremum

$$T_{1/2} = \frac{\Delta H}{\Delta S} \bigg|_{n_{\rm HS} = 1/2} \tag{7}$$

being the transition temperature that is reported from experiments. Notice that eq (7) shows that the equilibrium occurs for $n_{\rm HS} = 1/2$, meaning that there exists an equal population of low- and high-spin states at $T_{1/2}$. Both $\Delta E_{\rm sco}$ and $T_{1/2}$ from eqs (1) and (7), respectively, can be computed with the pySCO library as illustrated in Scheme 2.

In order to deepen our analysis to the microscopic picture of the spin conversion phenomenon, we now focus attention to the enthalpy and entropy differences in eq (6), ΔH and ΔS , respectively. These are expressed in terms of the thermal expansion $P \Delta V$, as well as

the electronic, vibrational and rotational contributions,

$$\Delta H = \Delta E_{\rm sco} + \Delta E_{\rm vib} + \Delta E_{\rm tra} + \Delta E_{\rm rot} + P \,\Delta V \tag{8}$$

$$\Delta S = \Delta S_{\text{ele}} + \Delta S_{\text{vib}} + \Delta S_{\text{tra}} + \Delta S_{\text{rot}} \tag{9}$$

These are obtained through the equations ^{56,57}

$$\Delta E_{\text{vib}} = k_B N_A \sum_{i \in \text{HS}} \left(\frac{\theta_{\text{vib}, i}}{e^{\theta_{\text{vib}, i}/T} - 1} \right) - k_B N_A \sum_{i \in \text{LS}} \left(\frac{\theta_{\text{vib}, i}}{e^{\theta_{\text{vib}, i}/T} - 1} \right)$$

$$\Delta S_{\text{vib}} = k_B N_A \sum_{i \in \text{HS}} \left(\frac{\theta_{\text{vib}, i}/T}{e^{\theta_{\text{vib}, i}/T} - 1} - \ln\left[1 - e^{\theta_{\text{vib}, i}/T}\right] \right) - k_B N_A \sum_{i \in \text{LS}} \left(\frac{\theta_{\text{vib}, i}/T}}{e^{\theta_{\text{vib}, i}/T} - 1} - \ln\left[1 - e^{\theta_{\text{vib}, i}/T}\right] \right)$$

$$(10)$$

In addition, the change in the electronic entropy $\Delta S_{\rm ele} = \Delta S_{\rm spin} + \Delta S_{\rm orb} + \Delta S_{\rm Fermi}$, is given by three contributions, namely, $\Delta S_{\rm spin} = k_B N_A \ln[~(1+2\,S_{\rm HS})/(1+2\,S_{\rm LS})~]$ that is associated with the change in the total spin S during the spin conversion, and the analogous expression for the entropy variation $\Delta S_{\rm orb}$ due to orbital angular momentum L.⁵⁸ The Fermi entropy difference, $\Delta S_{\rm Fermi}$, on the other hand, depends on the Fermi distribution $f(\varepsilon) = 1/(1+e^{\theta_{\rm Fermi}/T})$, with $\theta_{\rm Fermi} = (\varepsilon - \varepsilon_{\rm Fermi})/k_B$, where ε and $\varepsilon_{\rm Fermi}$ are the single-particle energy state and Fermi energy, respectively, for each spin state, so that

$$\Delta S_{\text{Fermi}} = -k_B N_A \int n(\varepsilon) (f(\varepsilon) \ln[f(\varepsilon)] + (1 - f(\varepsilon)) \ln[1 - f(\varepsilon)]) d\varepsilon \Big|_{\{\varepsilon\} \in \text{HS}}$$

$$+ k_B N_A \int n(\varepsilon) (f(\varepsilon) \ln[f(\varepsilon)] + (1 - f(\varepsilon)) \ln[1 - f(\varepsilon)]) d\varepsilon \Big|_{\{\varepsilon\} \in \text{LS}}$$
(12)

where $n(\varepsilon)$ is the electronic density of states.⁵⁹ It is worth noting that because the spin-switching metal complexes have a well-defined gap, ΔS_{Fermi} is expected to barely contribute to the computed $T_{1/2}$.

The changes for the translational contributions to the energy and entropy, ΔE_{tra} and ΔS_{tra} , respectively, and the rotational contribution to the energy, ΔE_{rot} , are sufficiently small that often are neglected. The rotational contribution to the entropy, ΔS_{rot} , on the other hand, is given by the expression

$$\Delta S_{\text{rot}} = k_B N_A \ln \left[\frac{1}{\sigma_r} \left(\frac{\pi T^3}{\theta_{r,x} \theta_{r,y} \theta_{r,x}} \right)^{1/2} \right]_{\{\sigma_r, \theta_r\} \in \text{HS}} - k_B N_A \ln \left[\frac{1}{\sigma_r} \left(\frac{\pi T^3}{\theta_{r,x} \theta_{r,y} \theta_{r,x}} \right)^{1/2} \right]_{\{\sigma_r, \theta_r\} \in \text{LS}}$$

$$(13)$$

where σ_r is the rotational symmetry number, and the set $\{\theta_r\}$ corresponds to the rotational temperatures that depend on the moment of inertia. ^{56,57}

It is clear from eqs (6) through (13) that $n_{\rm HS}$ and T, share a non-linear dependence. This means that we must evaluate numerically eq (6) to find $T_{1/2}$. For each choice of $n_{\rm HS}$ during the numerical procedure, one must also compute all temperature-dependent terms in ΔH and ΔS , while looping through the harmonic frequencies, $\{\nu\}$, in eqs (10) and (11), and single-particle energy states, $\{\varepsilon\}$, in eq (12) for both the low- and high-spin states. This is one of the main tasks of pySCO. It is handled automatically by the library without requiring user intervention.

We have discussed so far the basics of gradual spin conversions for weakly interacting molecules. Nonetheless, some highly cooperative materials with comparatively stronger intermolecular interaction exhibit rather abrupt spin switching. An energy barrier between the spin states hinders rapid thermal equilibration. This splits the heating, T_{\uparrow} , and cooling, T_{\downarrow} , transition temperatures into two distinct values separated by a finite hysteresis $\Delta T_{\uparrow\downarrow} = T_{\uparrow} - T_{\downarrow}$.

Slichter and Drickamer 60 proposed the addition of a non-linear mean field term independent of T to the regular solution model to parametrize that splitting in the form

$$G = (1 - n_{\rm HS}) G_{\rm LS} + n_{\rm HS} G_{\rm HS} + \Gamma n_{\rm HS} (1 - n_{\rm HS}) - T S_{\rm mix}$$
(14)

where the coefficient Γ for this second-order contribution in eq (14) is known as the phenomenological interaction parameter and, as the name suggests, accounts for the cooperative inter-molecular interactions. Analyzing the behavior of G during the spin transition, with both equations (3) or (14), is possible in the pySCO library for different isothermal profiles, as depicted in Scheme 3.

At this point, it is important to highlight the usefulness of the sign of Γ , namely, $\Gamma < 0$ is indicative that the molecules in the crystal prefer to be surrounded by other molecules with opposite spin, whereas the converse $\Gamma > 0$ is characteristic of molecules with preference for being enclosed by others with the same spin.

Scheme 3: Calculate the isothermal Gibbs free energy G as a function of the relative high-spin population $n_{\rm HS}$ using a fixed value for the phenomenological interaction parameter for low- and high-spin states defined as in Scheme 1.

Furthermore, the equilibrium condition for eq (14) is the same as in eq (5), but with the following expression for the thermal evolution of n_{HS} ,

$$T = \frac{\Delta H + \Gamma \left(1 - 2 n_{\text{HS}}\right)}{k_B N_A \ln \left[\frac{1 - n_{\text{HS}}}{n_{\text{HS}}}\right] + \Delta S}$$
(15)

Note that in this model, the hysteresis contribution vanishes for $n_{\rm HS} = 1/2$, and thus eq (15) reduces to eq (6) because the term $\Gamma(1 - 2 n_{\rm HS}) = 0 \mid_{n_{\rm HS}=1/2}$. Analogous to the previous code snippet, computing the thermally driven variation of $n_{\rm HS}$, with either eq (6) or (15),

using pySCO is exemplified in Scheme 4.

Scheme 4: Compute the relative high-spin population $n_{\rm HS}$ as a function of temperature T, without and with consideration of the phenomenological interaction parameter Γ , for low-and high-spin states defined as in Scheme 1.

Experimental determination of the interaction parameter usually is done with a nonlinear least squares fit to eq (15) to get an estimation for ΔH , ΔS , and Γ . The former two relate to $T_{1/2}$ through eq (7). Bear in mind that first-principles calculation of Γ has proven difficult to date, ^{27,29,61–66} both because of the complicated physical processes subsumed in its mean field, and because its magnitude is substantially smaller that $\Delta E_{\rm sco}$ which itself is computationally challenging. This phenomenological parameter results from averaging the different energy contributions to the inter-molecular interactions in a lattice and, in consequence, Γ may undergo sign flips during lattice relaxations of molecular crystals. ^{67,68}

To compute Γ with electronic structure methods, customarily one samples a series of different microscopic mixtures of low- and high-spin state configurations using super-cells. For instance, a unit cell with four metal centers has $2^4 = 16$ possible distributions, namely, one for $n_{\rm HS} = 0$ with all four being low-spin, and the opposite for $n_{\rm HS} = 1$; four for $n_{\rm HS} = 1/4$ with only one high-spin molecule, and four $n_{\rm HS} = 3/4$ for the converse; and finally six configurations for $n_{\rm HS} = 1/2$ with an equal mixture of molecules in both spin states. The total

```
from pysco import read
from pysco import thermo

mid_spins = []

configs = [ "LLLH", "LHLH", "HLHL", "HHHL" ]

low_spin = read.vasp( "LLLL_dir" )

high_spin = read.vasp( "HHHH_dir" )

for i in configs:
    mid_spins.append( read.vasp( f"{i}_dir" ) )

interaction, R = thermo.interaction_parameter(
    ls = low_spin,
    hs = high_spin,
    ms = mid_spins
)
```

Scheme 5: Compute the phenomenological interaction parameter Γ using a series of configuration choices sampling the interval $0.0 \le n_{\rm HS} \le 1.0$ in steps $\Delta n_{\rm HS} = 1/4$. For each unit cell, the generic labels L and H depict a metal center in a low- or high-spin state, respectively. As a result, $n_{\rm HS} = 0.0 \in \{\rm LLLL\}$, $n_{\rm HS} = 0.25 \in \{\rm LLLH\}$, $n_{\rm HS} = 0.5 \in \{\rm LHLH, HLHL\}$, $n_{\rm HS} = 0.75 \in \{\rm HHHL\}$, and $n_{\rm HS} = 1.0 \in \{\rm HHHH\}$.

number of possible distributions evidently becomes larger for progressively increasing supercells, but it may be reduced due to the presence of symmetry-related configurations. The results for these spin distributions are then used for fitting the interaction parameter.^{69–74} This is a straightforward method, illustrated in Scheme 5, with the pySCO library.

Computational Details

With the purpose of demonstrating the capabilities of the pySCO library, we focus attention on the homoleptic complex [Fe(tBu₂qsal)₂], with an average $T_{1/2} = 123$ K reported experimentally and characterized in ref 75. This metal complex is constituted by two tert-butyl substituents on one side of the adduct while leaving the other side free of steric hindrance that, arguably, helps increase the volatility of the material and, at the same time, preserve the strong elastic coupling between the neighboring molecules in the crystal. As a result, the material exhibits a hysteresis $\Delta T_{\uparrow\downarrow} = 12$ K, that is evidence of the strong cooperative behavior during the abrupt spin transition.

Before proceeding with the details pertaining to the electronic structure calculations for

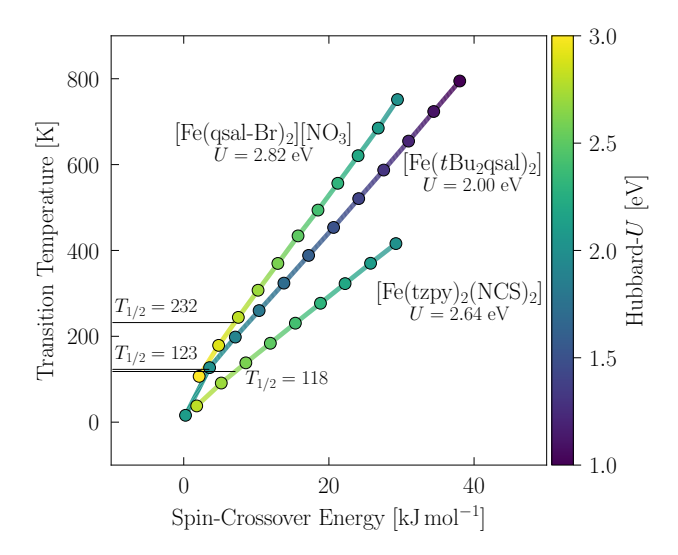


Figure 1: Variation of the transition temperature, $T_{1/2}$, and spin-crossover energy, $\Delta E_{\rm sco}$, as a function of the magnitude for the Hubbard-U correction. Results for the solid-state phases for the $[{\rm Fe}(t{\rm Bu_2qsal})_2]$, $[{\rm Fe}({\rm qsal-Br})_2][{\rm NO_3}]$, and $[{\rm Fe}(t{\rm zpy})_2({\rm NCS})_2]$ metal complexes are shown for comparison. The structures were taken from refs 75–77.

[Fe($tBu_2qsal)_2$], the reader should be aware that the choice of density functional approximation plays a crucial role in determining the quality of the results, as does the admixture of single-determinant exchange. ^{78–80} The analogous remains true for distinct choices of level of theory known for delivering qualitatively different trends, even for small spin-crossover archetypes. ^{81,82} For our study we chose periodic boundary conditions with the Vasp 6.3 code and the set of standard PBE potpaw.54 projector augmented wave potentials for Fe, O, N, C, and H that correspond to the valence electron configurations $3s^2 3p^6 3d^7 4s^1$, $2s^2 2p^4$, $2s^2 2p^3$, $2s^2 2p^2$, and $1s^1$, respectively. ⁴³ For the sake of consistency, the PBE generalized gradient exchange-correlation density functional approximation with the Hubbard-U correction also was selected. ^{83–86} The value U=2 eV was fitted as shown in Figure 1 to reproduce as close as possible the reported experimental transition temperature $T_{1/2}^{\text{expt}} = 123$ K for $[\text{Fe}(tBu_2qsal)_2]$. ⁷⁵ Note that the magnitude for U varies for different metal complexes, as illustrated in Figure 1 for $[\text{Fe}(tBu_2qsal)_2]$, $[\text{Fe}(qsal-Br)_2][\text{NO}_3]$ with $T_{1/2}^{\text{expt}} = 232$ K, ⁷⁷ and $[\text{Fe}(tzpy)_2(\text{NCS})_2]$ with $T_{1/2}^{\text{expt}} = 118$ K, ⁷⁶ with ligands $tBu_2qsal = 2,4$ -di(tert-butyl)-6-((quinoline-8-ylimino)methyl)phenol, qsal-Br = (N-8-quino-lyl)-5-Br-salicylaldiminate, and tzpy =

(3-(2-pyridyl)(1,2,3)triazolo(1,5-a)pyridine). The Hubbard-U magnitude is not transferable to a different choice of potential for the transition metal center.⁸⁷

In addition, the plane wave kinetic energy cutoff was set to 600 eV, with augmentation charges evaluated with an auxiliary support grid. Non-spherical corrections to the electron density gradient also were included. The threshold for the convergence of the self-consistent field was set to 10^{-9} eV, with a Gaussian smearing width of 10^{-2} eV. Furthermore, the coordinates for the solid-state materials were optimized with the conjugate gradient algorithm until forces were smaller than 10^{-3} eV Å⁻¹. A k-point density of 0.2 Å⁻¹ was used for this purpose, whereas solely the Gamma q-point was considered for phonon computations. These were done with a finite differences approach and a step size of 10^{-2} Å. Only the atoms through the first coordination shell for each of the Fe(II) centers in the unit cell were considered for the vibrational degrees of freedom. ^{88,89}

Treatment of the output files and thermodynamic analyses were done with the pySCO library. In addition, the thermal variation of the magnetic susceptibility obtained from the pySCO output depicted in Scheme 4 was approximated by

$$\mu_{S,L} = \sqrt{4S(S+1) + L(L+1)} \,\mu_B \tag{16}$$

where S and L are the total spin and spin momentum, respectively, and $\mu_B = 9.274 \text{ J T}^{-1}$ is the Bohr magneton. $\mu_{\text{S,L}}$ is then expressed as an ensemble average for the low- and high-spin states weighted by n_{HS} . ⁹⁰

The $[Fe(tBu_2qsal)_2]$ Metal Complex

Discussion of our results for the $[Fe(tBu_2qsal)_2]$ metal complex evidently must start with the key contribution to $T_{1/2}$ in eq (7), namely, ΔE_{sco} . As already stated, both quantities are readily available with pySCO following the procedure depicted in Scheme 2. We obtained a $\Delta E_{sco} = 3.21 \text{ kJ mol}^{-1}$ that is well within the expected energy range for spin-switching

materials. Though the calculated $T_{1/2} = 132$ K is nine units larger than the average experimental reference, the calculated value is close to the upper experimental limit $T_{1/2} = 123 \pm 6$ K. In the absence of reliable confidence limits on the calculated values, de facto this amounts to agreement with experiment.

With the $T_{1/2}$ validated, we proceed with the analysis of the thermal variation of the magnetic susceptibility, χT , following Scheme 4. For that it is necessary to compute the interaction parameter in eq (15) to model the hysteresis. In the interest of preserving a representative illustration, we considered the same subset of six spin distributions shown in Scheme 5. More specifically, the subset includes the pure low- and high-spin configurations, with $n_{\rm HS} = 0$ and $n_{\rm HS} = 1$, respectively, one for $n_{\rm HS} = 1/4$, two configurations for $n_{\rm HS} = 1/2$, and one for $n_{\rm HS} = 3/4$.

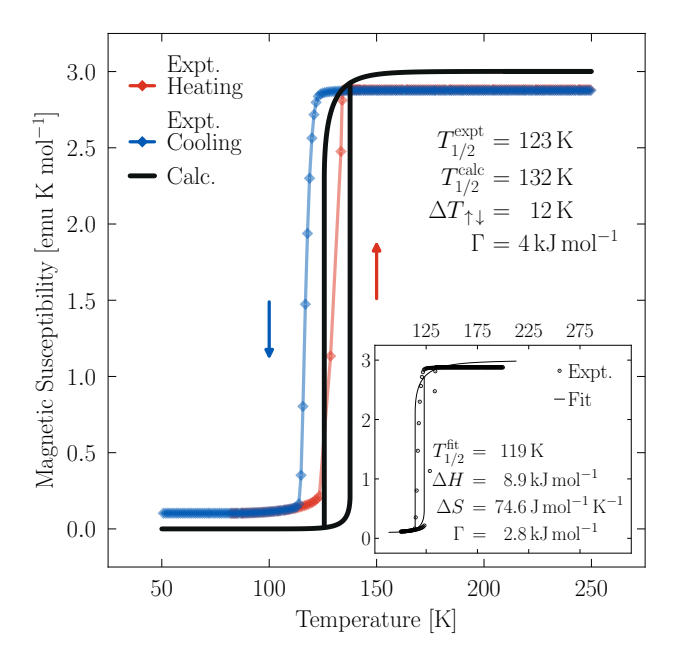


Figure 2: Comparison between the calculated and experimental transition temperature, $T_{1/2}$, and the temperature dependence of the magnetic susceptibility, χT , for $[\text{Fe}(t\text{Bu}_2\text{qsal})_2]$. The phenomenological interaction parameter, Γ , was fitted to reproduce the experimental hysteresis $\Delta T_{\uparrow\downarrow} = 12\,\text{K}$. On the other hand, the reference quantities reported in the inset correspond to the Slichter and Drickamer model fitted with the experimental data for χT taken from ref 75. The number of points shown in the inset were reduced to ease visualization.

The interaction parameter calculated with the procedure in Scheme 5 is $\Gamma = 2.28$

kJ mol⁻¹. However, that value yields no hysteresis. Details follow later in the discussion. As an aside, we resorted to fitting $\Gamma = 4$ kJ mol⁻¹ that reproduces the experimental hysteresis width. Results in Figure 2 show the agreement between the computed magnetic susceptibility with the experimental reference. We observe a shifted spin transition due to the 9 K overestimation for the calculated $T_{1/2}$ that leads to $\Delta H = 12.17$ kJ mol⁻¹ and $\Delta S = 92.0$ J mol⁻¹ K⁻¹. For comparison, the inset in Figure 2 shows the reference values $\Delta H = 8.9$ kJ mol⁻¹, $\Delta S = 74.6$ J mol⁻¹ K⁻¹, and $\Gamma = 2.8$ kJ mol⁻¹ that were extracted by fitting eq (15) to the experimental data. Both the predicted ΔH and ΔS agree reasonably well with the experiment, and eq (7) provides the basis to argue that the slight overestimation arises from the larger $T_{1/2}$ computed for the metal complex.

Details regarding the effects arising from the phenomenological interaction parameter, on the other hand, are better illustrated by monitoring the Gibbs free energy during the spin transition for the metal complex, described in Scheme 3. The spin conversion may be classified into three regimes depending on the sign of the second derivative of eq (14) around $T_{1/2}$,

$$\left(\frac{\partial^2 G}{\partial n_{\rm HS}^2}\right)_{T,P,n_{\rm HS}=1/2} = -2\Gamma + 4k_B N_A T_{1/2} \tag{17}$$

First are the weak interactions with $\partial^2 G/\partial n_{\rm HS}^2 > 0$ that result in gradual spin conversions if $\Gamma < 2 \, k_B \, N_A \, T_{1/2}$. It is the set of convex curves in Figure 3(a). Next is the critical point for which $\partial^2 G/\partial n_{\rm HS}^2 = 0$ with abrupt transitions if $\Gamma = 2 \, k_B \, N_A \, T_{1/2}$. It is highlighted in Figure 3(a) with the dotted line. This critical interaction for $[\text{Fe}(t \text{Bu}_2 \text{qsal})_2]$ is $2.2 \, \text{kJ} \, \text{mol}^{-1}$, close in magnitude to $\Gamma = 2.8 \, \text{kJ} \, \text{mol}^{-1}$ calculated previously and thus the reason for the absence of hysteresis with the latter. Then come the strong interactions with $\partial^2 G/\partial n_{\rm HS}^2 > 0$. It is the set of concave curves shown in Figure 3(a). Often this case involves first-order phase transitions and hysteresis, 8,91 with cooling T_{\downarrow} , transition $T_{1/2}$, and heating T_{\uparrow} temperatures, each with associated Gibbs free energy minimum, $G_{\rm min}$, as shown in Figure 3(b). The possibility of observing three $n_{\rm HS}$ values for a $T_{\downarrow} \leq T \leq T_{\uparrow}$ is well established for this regime. These may be related to stable, metastable or unstable spin configurations. See refs 92 and 65 for

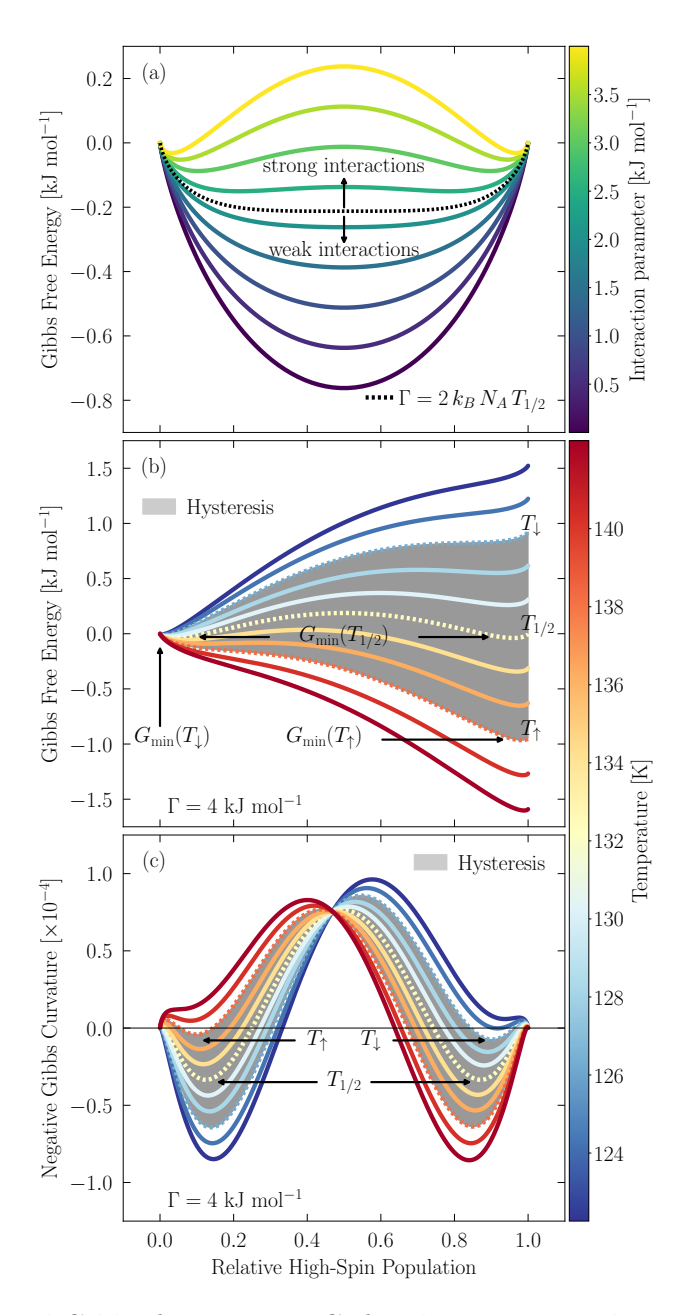


Figure 3: (a) Isothermal Gibbs free energy, G, for the progressively increasing relative highspin population, $n_{\rm HS}$, for different choices of the phenomenological interaction parameter, Γ . The critical point $\Gamma = 2 \, k_B \, N_A \, T_{1/2}$ delimits the region between weakly and strongly interacting molecules. All the isotherms are for the computed transition temperature $T_{1/2} = 132 \, {\rm K}$. (b) Gibbs free energy as a function of the relative high-spin population for different choices of temperature at fixed $\Gamma = 4 \, {\rm kJ} \,$ mol $^{-1}$. Three isotherms are highlighted, namely, T_{\downarrow} , $T_{1/2}$, and T_{\uparrow} , that correspond to the cooling, transition, and heating temperature, respectively. (c) $-(\partial^2 G/\partial n_{\rm HS}^2)_{T,P}$ for various temperatures. The shaded area in panels (b) and (c) depicts the hysteresis temperature interval $T_{\downarrow} \leq T \leq T_{\uparrow}$, whereas the dotted lines depict the cooling, transition, and heating temperature T_{\downarrow} , $T_{1/2}$, and T_{\uparrow} , respectively.

detailed discussions.

A more detailed analysis of the hysteresis regime, $T_{1/2} \pm 6$ K, for $[\text{Fe}(t\text{Bu}_2\text{qsal})_2]$ can be done by means of a series of isotherms for $-(\partial^2 G/\partial n_{\text{HS}}^2)_{T,P}$, as depicted in Figure 3(c). The negative Gibbs curvature shows favorable minima near $n_{\text{HS}} = 0$ and unfavorable near $n_{\text{HS}} = 1$ for $T < T_{\downarrow}$. The converse is observed for $T > T_{\uparrow}$. This is the typical behavior during spin conversion, namely, low temperatures favor the low-spin state, whereas high temperatures favor the high-spin state. For the hysteresis temperature interval, $T_{\downarrow} \leq T \leq T_{\uparrow}$, on the other hand, the existence of two minima is evident in Figure 3(c). In further detail, notice that there are meta stable high-spin states near $n_{\text{HS}} = 0$ for $T_{\downarrow} \leq T < T_{1/2}$, whereas the presence meta stable low-spin states near $n_{\text{HS}} = 1$ is observed for $T_{1/2} < T \leq T_{\uparrow}$. At the transition temperature, $T_{1/2}$, we can see in Figure 3(c) that there are two equally favorable minima near both the vicinities of $n_{\text{HS}} = 0$ and $n_{\text{HS}} = 1$. These minima are blocked energetically in the hysteresis temperature regime and, as a result, the metal complex may remain partially trapped in either spin state. A relatively slow relaxation towards the more stable spin state depends upon a delicate balance between temperature and the energy barrier height.

Lastly, it is worth noting that the experimental interaction parameter $\Gamma=2.8 \text{ kJ} \text{ mol}^{-1}$ for $[\text{Fe}(t\text{Bu}_2\text{qsal})_2]$ is close in magnitude to the 1.97, 2.30, and 2.97 kJ mol⁻¹ reported ⁹³ for $[\text{Fe}(\text{btz})_2(\text{NCS})_2]$, ⁹⁴ $[\text{Fe}(\text{bpz})_2(\text{bipy})_2]$, ⁹⁵ and $[\text{Fe}(\text{phen})_2(\text{NCS})_2]$, ⁹⁶ respectively, with ligands phen = 1,2-phenanthroline, btz = 5,5',6,6'-tetrahydro-4*H*,4'*H*-2-2'-bi-1,3-thiazine, dpz = dihydrobis(1-pyrazolil)borate, and bipy = 2,2'-bipyridine. All these metal complexes share somewhat similar asymmetric steric hindrance and are considered attractive for use in sublimation techniques to fabricate thin films, ⁹ which confirms the importance of understanding the influence of different choices of ligands upon the inter-molecular interactions for these materials.

Concluding Remarks

In summary, we introduced the pySCO library that allows for conducting high-throughput scalable analyses with greater ease, facilitating the study of the spin conversion phenomenon in molecules and solid state materials. By showcasing its use on the $[Fe(tBu_2qsal)_2]$ metal complex, we discussed the influence of the phenomenological interaction parameter using the mean field regular solution model available in the library. Our results served to provide a detailed examination of the interaction regimes for this complex. These are in part responsible for the volatility characteristics in asymmetric metal complexes, which are of interest for the preparation of ultra thin interface heterostructures.

Data and Software Availability

The pySCO library is an open source project and is available for download in the public repository github.com/amalbavera/pysco. ¹ The library uses the International System of Units, therefore, the spin conversion energy $\Delta E_{\rm sco}$, the enthalpy ΔH , and the phenomenological interaction parameter Γ are in kJ mol⁻¹, whereas the temperature T is in Kelvin, and the entropy ΔS in J mol⁻¹ K⁻¹. The repository also collects the VASP output files for the [Fe(tBu₂qsal)₂] metal complex needed for the calculation of the spin crossover energy, transition temperature, and analyses for the phenomenological interaction parameter. A Jupyter notebook also is included with illustrative code blocks to reproduce the results.

Acknowledgement

The author is grateful to S.B. Trickey, Richard G. Hennig, and Xiao-Guang Zhang for the constructive discussions and their insightful remarks. This work was supported as part of the Center for Molecular Magnetic Quantum Materials, an Energy Frontier Research

¹The pySCO code will be made public during publication of the manuscript. The VASP output files and Jupyter Notebook already are available

Center funded by the U.S. Department of Energy, Office of Science, Basic Energy Sciences under Award No. DE-SC0019330. This research used resources of the National Energy Research Scientific Computing Center (NERSC), a Department of Energy Office of Science User Facility using NERSC award BES-ERCAP0022828.

References

- (1) Gütlich, P.; Ksenofontov, V.; Gaspar, A. B. Pressure effect studies on spin crossover systems. *Coord. Chem. Rev.* **2005**, *249*, 1811–1829.
- (2) Bousseksou, A.; Molnár, G.; Salmona, L.; Nicolazzi, W. Molecular spin crossover phenomenon: recent achievements and prospects. *Chem. Soc. Rev.* **2011**, *40*, 3313–3335.
- (3) Gaspar, A. B.; Seredyuk, M. Spin crossover in soft matter. *Coord. Chem. Rev.* **2014**, 268, 41–58.
- (4) Hogue, R. W.; Singh, S.; Brooker, S. Spin crossover in discrete polynuclear iron(II) complexes. *Chem. Soc. Rev.* **2018**, *47*, 7303–7338.
- (5) Brady, C.; McGarvey, J. J.; McCusker, J. K.; Toftlund, H.; Hendrickson, D. N. Time-Resolved Relaxation Studies of Spin Crossover Systems in Solution. *Top. Curr. Chem.* 2004, 235, 1–22.
- (6) Rodríguez-Jiménez, S.; Brooker, S. Solid Versus Solution Spin Crossover and the Importance of the Fe-N≡C(X) Angle. *Inorg. Chem.* 2017, 56, 13697–13708.
- (7) Wang, J.; Li, Y.; Wei, R.-J.; Tang, Z.; Yao, Z.-S.; Tao, J. Spin-Crossover Behaviors of Iron(II) Complexes Bearing Halogen Ligands in Solid State and Solution. *Inorg. Chem.* 2023, 62, 1354–1361.
- (8) Ridier, K.; Molnár, G.; Salmon, L.; Nicolazzi, W.; Bousseksou, A. Hysteresis, nucleation and growth phenomena in spin-crossover solids. *Solid State Sci.* **2017**, *74*, A1–A22.

- (9) Kumar, K. S.; Ruben, M. Sublimable Spin-Crossover Complexes: From Spin-State Switching to Molecular Devices. *Angew. Chem. Int. Ed.* **2021**, *60*, 7502–7521.
- (10) Kipgen, L.; Bernien, M.; Tuczek, F.; Kuch, W. Spin-Crossover Molecules on Surfaces: From Isolated Molecules to Ultrathin Films. *Adv. Mater.* **2021**, *33*, 2008141.
- (11) Amin, N. A. A. M.; Said, S. M.; Salleh, M. F. M.; Afifi, A. M.; Ibrahim, N. M. J. N.; Hasnan, M. M. I. M.; Tahir, M.; Hashim, N. Review of Fe-based spin crossover metal complexes in multiscale device architectures. *Inorg. Chim. Acta* 2023, 544, 121168.
- (12) Yazdani, S.; Phillips, J.; Ekanayaka, T. K.; Cheng, R.; Dowben, P. A. The Influence of the Substrate on the Functionality of Spin Crossover Molecular Materials. *Molecules* **2023**, *28*, 3735.
- (13) Kahn, O. Molecular Magnetism; VCH Publishers Inc.: New York, 1993.
- (14) Jean, Y. Molecular Orbitals of Transition Metal Complexes; Oxford University Press: New York, 2005.
- (15) Mohn, P. Magnetism in the Solid State; Springer-Verlag: Berlin Heidelberg, 2006.
- (16) Dimian, M.; Rotaru, A. In *Magnetic Materials*; Maaz, K., Ed.; IntechOpen: Rijeka, 2016; Chapter 5.
- (17) Gütlich, P.; Goodwin, H. A. Spin crossover in transition metal compounds; Springer: Berlin: New York, 2004.
- (18) Gütlich, P.; Goodwin, H. A. Spin crossover in transition metal compounds I; Springer: Berlin: Heidelberg, 2004; pp 1–47.
- (19) Gütlich, P.; Goodwin, H. A. Spin crossover in transition metal compounds II; Springer: Berlin: Heidelberg, 2004.

- (20) Létard, J.-F.; Guionneau, P.; Goux-Capes, L. In *Spin Crossover in Transition Metal Compounds III*; Gütlich, P., Goodwin, H. A., Eds.; Springer: Berlin: Heidelberg, 2004; pp 221–249.
- (21) Polanyi Colloquium im Kaiser Wilhelm-Institut für physikalische Chemie und Elektrochemie. Ztschr. angew. Chem. 1931, 44, 207–208.
- (22) Cambi, L.; Szegö, L. Über die magnetische Susceptibilität der komplexen Verbindungen. Ber. Dtsch. Chem. Ges. 1931, 64, 2591–2598.
- (23) Baker, W. A.; Bobonich, H. M. Magnetic Properties of Some High-Spin Complexes of Iron(II). *Inorg. Chem.* **1964**, *3*, 1184–1188.
- (24) König, E.; Madeja, K. Unusual magnetic behaviour of some iron(II)-bis-(1,10-phenanthroline) complexes. *Chem. Commun.* **1966**, 61–62.
- (25) Wajnflasz, J. Etude de la transition "Low Spin"-"High Spin" dans les complexes octaédriques d'ion de transition. *Phys. Stat. Sol.* **1970**, *40*, 537–545.
- (26) Wajnflasz, J.; Pick, R. Transitions Low Spin High Spin dans les Complexes de Fe²⁺.

 J. Phys. Collog. 1971, 32, 90–91.
- (27) Boča, R.; Linert, W. Is There a Need for New Models of the Spin Crossover? *Montash. Chem.* **2003**, *134*, 199–216.
- (28) Koudriavtsev, A. B.; Linert, W. Spin Crossover an Unusual Chemical Equilibrium. *J. Struct. Chem.* **2010**, *51*, 335–365.
- (29) Pavlik, J.; Boŏa, R. Established Static Models of Spin Crossover. Eur. J. Inorg. Chem. 2013, 2013, 697–709.
- (30) Gaspar, A. B.; Ksenofontov, V.; Seredyuk, M.; Gütlich, P. Coord. Chem. Rev. 2005, 249, 2661–2667.

- (31) Gaspar, A. B.; Seredyuk, M.; Gütlich, P. Spin crossover in metallomesogens. *Coord. Chem. Rev.* **2009**, *253*, 2399–2413.
- (32) Gaspar, A. B.; Seredyuk, M.; Gütlich, P. Spin crossover in iron(II) complexes: Recent advances. J. Mol. Struc. 2009, 924–926, 9–19.
- (33) Atmani, C.; Hajj, F. E.; Benmansour, S.; Marchivie, M.; Triki, S.; Conan, F.; Patinec, V.; Handel, H.; Dupouy, G.; Gómez-García, C. J. Guidelines to design new spin crossover materials. *Coord. Chem. Rev.* **2010**, *254*, 1559–1569.
- (34) Harding, D. J.; Harding, P.; Phonsri, W. Spin crossover in iron(III) complexes. *Coord. Chem. Rev.* **2016**, *313*, 38–61.
- (35) Ferrando-Soria, J.; Vallejo, J.; Castellano, M.; Martínez-Lillo, J.; Pardo, E.; Cano, J.; Castro, I.; Lloret, F.; Ruiz-Garcia, R.; Julve, M. Molecular magnetism, quo vadis? A historical perspective from a coordination chemist viewpoint. Coord. Chem. Rev. 2017, 339, 17–103.
- (36) Wang, M.; Li, Z.-Y.; Ishikawa, R.; Yamashita, M. Spin crossover and valence tautomerism conductors. *Coord. Chem. Rev.* **2021**, *435*, 213819.
- (37) Tao, J.; Wei, R.-J.; Huang, R.-B.; Zheng, L.-S. Polymorphism in spin-crossover systems. *Chem. Soc. Rev.* **2012**, *41*, 703–737.
- (38) Collet, E.; Guionneau, P. Structural analysis of spin-crossover materials: From molecules to materials. C. R. Chimie 2018, 21, 1133–1151.
- (39) Matouzenko, G. S.; Bousseksou, A.; Lecocq, S.; van Koningsbruggen, P. J.; Perrin, M.; Kahn, O.; Collet, A. Polymorphism in Spin Transition Systems. Crystal Structure, Magnetic Properties, and Mo1 ssbauer Spectroscopy of Three Polymorphic Modifications of [Fe(DPPA)(NCS)2] [DPPA) (3-Aminopropyl)bis(2-pyridylmethyl)amine]. *Inorg. Chem.* 1997, 36, 5869–5879.

- (40) Frisch, M. J.; at al. Gaussian. 2016; Gaussian Inc. Wallingford CT.
- (41) Valiev, M.; et al. NWChem: A comprehensive and scalable open-source solution for large scale molecular simulations. *Comput. Phys. Commun.* **2010**, *181*, 1477.
- (42) Neese, F. Software update: The ORCA program system—Version 5.0. WIRES Comput. Molec. Sci. 2022, 12, e1606.
- (43) Kresse, G.; Furthmüller, J. Efficient Iterative Schemes for Ab Initio Total-Energy Calculations Using a Plane-Wave Basis Set. *Phys. Rev. B* **1996**, *56*, 11169.
- (44) Giannozzi, P.; et al. Advanced capabilities for materials modelling with QUANTUM ESPRESSO. J. Phys. Condens. Matter 2017, 29, 465901.
- (45) König, E. Nature and dynamics of the spin-state interconversion in metal complexes. Complex Chemistry. Berlin, Heidelberg, 1991; pp 51–152.
- (46) Bousseksou, A.; Nasser, J.; Linares, J.; Boukheddaden, K.; Varret, F. Ising-like model for the two-step spin-crossover. *J. Phys. I France* **1992**, *2*, 1381–1403.
- (47) Bousseksou, A.; Varret, F.; Nasser, J. Ising-like model for the two step spin-crossover of binuclear molecules. *J. Phys. I France* **1993**, *3*, 1463–1473.
- (48) Linares, J.; Nasser, J.; Bousseksou, A.; Boukheddaden, K.; Varret, F. Monte Carlo simulations of spin-crossover transitions using the two-level model. I: Mononuclear single sublattice case. J. Mag. Mag. Mater 1995, 140–144, 1503–1504.
- (49) Linares, J.; Nasser, J.; Bousseksou, A.; Boukheddaden, K.; Varret, F. Monte Carlo simulations of spin-crossover transitions using the two level model. II: Binuclear case. J. Mag. Mag. Mater 1995, 140–144, 1507–1508.
- (50) Stoleriu, L.; Chakraborty, P.; Hauser, A.; Stancu, A.; Enachescu, C. Thermal hysteresis in spin-crossover compounds studied within the mechanoelastic model and its potential application to nanoparticles. *Phys. Rev. B* **2011**, *84*, 134102.

- (51) Nicolazzi, J. P. W.; Molnár, G.; Boŏa, R.; Bousseksou, A. Coupled magnetic interactions and the Ising-like model for spin crossover in binuclear compounds. *Eur. Phys. J. B* **2013**, *86*, 292.
- (52) Mikolasek, M.; Nicolazzi, W.; Terki, F.; Molnár, G.; Bousseksou, A. Investigation of surface energies in spin crossover nanomaterials: the role of surface relaxations. *Phys. Chem. Chem. Phys.* **2017**, *19*, 12276–12281.
- (53) Markin, O.; Gudyma, I.; Boukheddaden, K. Role of harmonic and anharmonic interactions in controlling the cooperativity of spin-crossover molecular crystals. *Phys. Rev.* B 2024, 110, 174416.
- (54) Hildebrand, J. H.; Scott, R. L. Regular Solutions; Prentice-Hall international series in chemistry; Prentice-Hall, 1962.
- (55) Hildebrand, J. H.; Prausnitz, J. M.; Scott, R. L. Regular and related solutions: the solubility of gases, liquids, and solids; Van Nostrand Reinhold Co.: New York, 1970.
- (56) McQuarrie, D. A. Statistical Mechanics; Harper and Row: New York, 1976; pp 35–64.
- (57) McQuarrie, D. A.; Simon, J. D. *Molecular Thermodynamics*; University Science Books: Sausalito CA, 1999; pp 143–168.
- (58) Quintano, M. M.; Silva, M. X.; Belchior, J. C.; Braga, J. P. Electronic Entropy as a Periodic Property of the Elements: A Theoretical Chemistry Approach. J. Chem. Ed. 2021, 98, 2574–2577.
- (59) Nicholson, D. M. C.; Stocks, G. M.; Wang, Y.; Shelton, W. A.; Szotek, Z.; Temmerman, W. M. Stationary nature of the density-functional free energy: Application to accelerated multiple-scattering calculations. *Phys. Rev. B* **1994**, *50*, 14686(R).
- (60) Slichter, C. P.; Drickamer, H. G. Pressure-Induced Electronic Changes in Compounds of Iron. J. Chem. Phys. 1972, 56, 2142–2160.

- (61) Boukheddaden, K.; Shteto, I.; Hôo, B.; Varret, F. Dynamical model for spin-crossover solids. I. Relaxation effects in the mean-field approach. *Phys. Rev. B* **2000**, *62*, 14796.
- (62) Boukheddaden, K.; Shteto, I.; Hôo, B.; Varret, F. Dynamical model for spin-crossover solids. II. Static and dynamic effects of light in the mean-field approach. *Phys. Rev. B* 2000, 62, 14806.
- (63) Kepenekian, M.; Guennic, B. L.; Robert, V. Magnetic bistability: From microscopic to macroscopic understandings of hysteretic behavior using ab initio calculations. *Phys. Rev. B* 2009, 79, 094428.
- (64) Enachescu, C.; Nicolazzi, W. Elastic models, lattice dynamics and finite size effects in molecular spin crossover systems. *Comptes Rendus. Chimie* **2018**, *21*, 1179–1195.
- (65) Nicolazzi, W.; Bousseksou, A. Thermodynamical aspects of the spin crossover phenomenon. C. R. Chimie 2018, 21, 1060–1074.
- (66) Collet, E.; Azzolina, G. Coupling and decoupling of spin crossover and ferroelastic distortion: Unsymmetric hysteresis loop, phase diagram, and sequence of phases. *Phys. Rev. Mater.* 2021, 5, 044401.
- (67) Tchougréeff, A. L. Lattice Relaxation and Cooperativity in the Low-Spin to High-Spin Transitions in Molecular Crystals. *Mol. Cryst. Liq. Cryst.* **1995**, *274*, 17–23.
- (68) Tchougréeff, A. L.; Darkhovskii, M. B. Lattice relaxation and order in the low-spin to high-spin transitions in molecular crystals. *Int. J. Quantum Chem.* **1996**, *57*, 903–912.
- (69) Paulsen, H. Periodic Density Functional Calculations in Order to Assess the Cooperativity of the Spin Transition in Fe(phen)₂(NCS)₂. Magnetochemistry **2016**, 2, 14.
- (70) De, S.; Tewary, S.; Garnier, D.; Li, Y.; Gontard, G.; Lisnard, L.; Flambard, A.; Breher, F.; Boillot, M.-L.; Rajaraman, G.; Lescouëzec, R. Solution and Solid-State Study

- of the Spin-Crossover $[Fe^{II}(R-bik)_3](BF4)_2$ Complexes (R = Me, Et, Vinyl). Aur. J. Org. Chem. **2018**, 2018, 208–543.
- (71) Vela, S.; Paulsen, H. Cooperativity in Spin Crossover Systems. An Atomistic Perspective on the Devil's Staircase. *Inorg. chem.* **2018**, *57*, 9478–9488.
- (72) Pillet, S. Spin-crossover materials: Getting the most from x-ray crystallography. *J. Appl. Phys.* **2021**, *129*, 181101.
- (73) Popa, A.-I.; Stoleriu, L.; Enachescu, C. Tutorial on the elastic theory of spin crossover materials. *J. Appl. Phys.* **2021**, *129*, 131101.
- (74) Wolny, J. A.; Gröpl, K.; Kiehl, J.; Rentschler, E.; Schünemann, V. Quantification of the thermodynamic effects of the low-spin high-spin interaction in molecular crystals of a mononuclear iron(ii) spin crossover complex. *Dalton Trans.* **2024**, *53*, 8391–8397.
- (75) Gakiya-Teruya, M.; Jiang, X.; Le, D.; Üngör, Ö.; Durrani, A. J.; Koptur-Palenchar, J. J.; Jiang, J.; Jiang, T.; Meisel, M. W.; Cheng, H.-P.; Zhang, X.-G.; Zhang, X.-X.; Rahman, T. S.; Hebard, A. F.; Shatruk, M. Asymmetric Design of Spin-Crossover Complexes to Increase the Volatility for Surface Deposition. *J. Am. Chem. Soc.* **2021**, *143*, 14563–14572.
- (76) Niel, V.; Gaspar, A. B.; Muñoz, M. C.; Abarca, B.; Ballesteros, R.; Real, J. A. Spin Crossover Behavior in the Iron(II)-2-pyridyl[1,2,3]triazolo[1,5-a]pyridine System: X-ray Structure, Calorimetric, Magnetic, and Photomagnetic Studies. *Inorg. Chem.* **2003**, 42, 4782–4788.
- (77) Harding, D. J.; Phonsri, W.; Harding, P.; Murray, K. S.; Moubaraki, B.; Jameson, G. N. L. Abrupt two-step and symmetry breaking spin crossover in an iron(iii) complex: an exceptionally wide [LS-HS] plateau. *Dalton Trans.* 2015, 44, 15079–15082.

- (78) Radoń, M. Revisiting the role of exact exchange in DFT spin-state energetics of transition metal complexes. *Phys. Chem. Chem. Phys.* **2014**, *16*, 14479–14488.
- (79) Kepp, K. P. Theoretical Study of Spin Crossover in 30 Iron Complexes. *Inorg. Chem.* **2016**, *55*, 2717–2727.
- (80) Kepp, K. P. In Transition Metals in Coordination Environments: Computational Chemistry and Catalysis Viewpoints; Broclawik, E., Borowski, T., Radoń, M., Eds.; Springer International Publishing: Cham, 2019; pp 1–33.
- (81) Song, S.; Kim, M.-C.; Sim, E.; Benali, A.; Heinonen, O.; Burke, K. Benchmarks and Reliable DFT Results for Spin Gaps of Small Ligand Fe(II) Complexes. *J. Chem. Theory Comput.* **2018**, *14*, 2304–2311.
- (82) Phung, Q. M.; Feldt, M.; Harvey, J. N.; Pierloot, K. Toward Highly Accurate Spin State Energetics in First-Row Transition Metal Complexes: A Combined CASPT2/CC Approach. J. Chem. Theory Comput. 2018, 14, 2446–2455.
- (83) Perdew, J. P.; Burke, K.; Ernzerhof, M. Generalized Gradient Approximation Made Simple. *Phys. Rev. Lett* **1996**, *77*, 3865.
- (84) Perdew, J. P.; Burke, K.; Ernzerhof, M. Generalized Gradient Approximation Made Simple [Phys. Rev. Lett. 77, 3865 (1996)]. Phys. Rev. Lett 1997, 78, 1396.
- (85) Dudarev, S. L.; Botton, G. A.; Savrasov, S. Y. Electron-Energy-Loss Spectra and the Structural Stability of Nickel Oxide: An LSDA+U Study. *Phys. Rev. B* **1998**, *57*, 1505.
- (86) Tolba, S. A.; Gameel, K. M.; Ali, B. A.; Almossalami, H. A.; Allam, N. K. In *Density Functional Calculations*; Yang, G., Ed.; IntechOpen: Rijeka, 2018; Chapter 1.
- (87) Albavera-Mata, A.; Hennig, R. G.; Trickey, S. Mean Value Ensemble Hubbard-U Correction for Spin-Crossover Molecules. J. Phys. Chem. Lett. 2022, 13, 12049–12054.

- (88) Albavera-Mata, A.; Hennig, R. G.; Trickey, S. Transition Temperature for Spin-Crossover Materials with the Mean Value Ensemble Hubbard-U Correction. *J. Phys. Chem. A* **2023**, *127*, 7646–7654.
- (89) Albavera-Mata, A.; Liu, S.; Cheng, H.-P.; Hennig, R. G.; Trickey, S. Magnetic and Thermodynamic Computations for Supramolecular Assemblies between a Cr(III) and Fe(III) Single-Ion Magnet and an Fe(II) Spin-Crossover Complex. J. Phys. Chem. A 2024, 128, 10929–10935.
- (90) Mugiraneza, S.; Hallas, A. M. Tutorial: a beginner's guide to interpreting magnetic susceptibility data with the Curie-Weiss law. *Commun. Phys.* **2022**, *5*, 95.
- (91) Halcrow, M. A. Spin-Crossover Materials; John Wiley & Sons, Ltd, 2013; Chapter 5, pp 147–169.
- (92) Brooker, S. Spin crossover with thermal hysteresis: practicalities and lessons learnt. *Chem. Soc. Rev.* **2015**, *44*, 2880–2892.
- (93) Sinitskiy, A. V.; Tchougréeff, A. L.; Dronskowski, R. Phenomenological model of spin crossover in molecular crystals as derived from atom–atom potentials. *Phys. Chem. Chem. Phys.* **2011**, *13*, 13238–13246.
- (94) Real, J. A.; Gallois, B.; Granier, T.; Suez-Panama, F.; Zarembowitch, J. Comparative investigation of the spin-crossover compounds Fe(btz)₂(NCS)₂ and Fe(phen)₂(NCS)₂ (where btz = 2,2'-bi-4,5-dihydrothiazine and phen = 1,10-phenanthroline). Magnetic properties and thermal dilatation behavior and crystal structure of Fe(btz)₂(NCS)₂ at 293 and 130 K. *Inorg. Chemm* **1992**, *31*, 4972–4979.
- (95) Real, J. A.; Muñoz, M. C.; Faus, J.; Solans, X. Spin Crossover in Novel Dihydrobis(1-pyrazolyl)borate [H₂B(pz)₂]-Containing Iron(II) Complexes. Synthesis, X-ray Structure, and Magnetic Properties of [FeL{H₂B(pz)₂}₂] (L = 1,10-Phenanthroline and 2,2'-Bipyridine). Inorg. Chem. 1997, 36, 3008–3013.

(96) Gallois, B.; Real, J.-A.; Hauw, C.; Zarembowitch, J. Structural changes associated with the spin transition in bis(isothiocyanato)bis(1,10-phenanthroline)iron: a single-crystal x-ray investigation. *Inorg. Chem.* **1990**, *29*, 1152–1158.

TOC Graphic

